Developments in Drag Reduction Methods and Devices for Road Vehicles

Michael Gerard Connolly*, Alojz Ivankovic and Malachy J. O'Rourke
University College Dublin, Dublin, Ireland

***michael.connolly@ucdconnect.ie**

This work is derived from material originally published in "Developments in Drag Reduction Methods and Devices for Road Vehicles" by Connolly, M. G.; Ivankovic, A.; O'Rourke, M. J., Applied Sciences, 2025 (DOI: 10.3390/app15179693) [1].

Abstract

This study presents new developments into novel drag reduction devices for road vehicles, focusing on the use of inflatable and alternative material rear drag reduction devices that employ both a single and multi cavity approach. The effectiveness of these devices is assessed through on-road testing using constant power measurements to evaluate the resulting drag reductions. Surface pressure measurements collected during testing are compared with CFD predictions, using both RANS and HLES methods to evaluate how accurately pressure changes are modelled when the devices are fitted to the test vehicles. A novel method for analysing vehicle surface flow in real-world conditions is also introduced, involving the capture and processing of video-recorded tuft imagery to determine appropriate means and standard deviations for the surface flow behaviour.

1 Introduction

The need for improved fuel economy and drag reduction in the road transport sector has become critical once again as it was following the oil crisis of the 1970s [2]. This renewed urgency is driven by many factors, which include the ongoing climate crisis [3], the demand for improved electric vehicle driving range [4], and the volatility of fuel prices due to geopolitical situations [5]. One of the most effective ways to improve a vehicle's fuel economy is to reduce the air resistance forces it experiences when on the road. Once a passenger car exceeds a speed of approximately 60 km/h, aerodynamic drag becomes the largest resistance force the vehicle must overcome [6]. The main issue is that the power requirement to overcome this air resistance grows in proportion to the cube of the vehicle's speed, which is one of the primary causes of why substantial fuel economy and range detriments are observed when driving at typical motorway speeds (120 km/h) [7]. Reducing aerodynamic drag on a vehicle reduces fuel consumption; however, the relationship between these reductions is highly dependent on a number of factors, such as vehicle type and driving cycle [6]. In general, when any road vehicle conducts a high-speed long-distance journey, drag is the largest consumer of the fuel used for that journey. A reasonable estimate, commonly used for such a driving cycle, is that a 10% drag reduction would realise a 5% fuel saving [8] [9] [10]. If the driving cycle was different, such as incorporating more city-based or outer city driving, which includes accelerations, starts and stops, then the weighting can be reduced to below 5% [11]. At the higher road speeds (100–120 km/h), aerodynamic drag can significantly exceed rolling resistance, making drag reduction one of the most effective strategies for improving fuel economy and addressing the current needs and challenges in the road transport sector.

2 Literature Review

The rear of a vehicle is particularly well suited for the addition of aerodynamic devices, due to the significant drag caused by the low-pressure wake that forms after flow separation at the end of a bluff body [12]. A comprehensive review of rear and other vehicle-mounted drag-reduction devices was presented in [13], which summarised key developments in the field over the past 50 years. The findings relevant to the present work are summarised next.

A wide variety of rear drag reduction strategies has been assessed in the literature, with performance depending on the shape and size of the device along with the vehicle type. [14] demonstrated a device known as the fluid tail, which redirected air from the rear wheel arches into the rear wake, reducing drag by 18–20% on a production hatchback, while [15] integrated servo-actuated flaps into a base cavity on an SUV to improve yaw-averaged drag performance. [16] outlined work related to the development of an inflatable rear drag reduction device for a road vehicle. The paper outlined drag reduction results for a very simplified body using scale wind tunnel work, without full-scale prototyping or results for the inflatable device on a passenger car. [17] showed that inward-angled deflectors at 20 degrees significantly diminished wake turbulence on a square-back configuration. [18] demonstrated that a tapered rear cavity could more than double the drag reduction achieved by a straight cavity in direct flow. Streamlined tail extensions were studied in [19], reporting up to 60% drag reductions using elongated, tapered designs, which maintained most of the drag reduction performance when truncated. Similarly, [20] showed that truncating a full boat tail on a box van yielded only a marginal performance drop, with drag reductions falling to just 31% from 32%. [21] measured a 3.3% drag reduction with a recessed cavity on an SUV without passive base bleeding, with only a 1% extra performance improvement when the base bleeding was included, highlighting how the initial cavity contributed most of the savings. [12] presented a new type of rear drag reduction device, known as the multi-stage converging cavity, which utilised multiple angled cavities within one another to access a downstream high-pressure zone. The device then redistributed this pressure over the vehicle's base, realising substantial base drag reductions.

In the context of heavy-duty vehicles, [22] examined a boat tail design with a shortened, angled bottom panel and found that excluding the bottom panel halved the overall drag reduction, underscoring the need for bottom surfaces on rear cavities and tails. A study by [23] confirmed that increased cavity length enhanced drag reduction, especially when combined with side skirts, with [24] documenting a 6.5% fuel saving for a road-tested practical cavity device on a heavy truck. Various appendables were studied in [25] for a pick-up truck, where combining a rear boat tail constructed from plates with a partial bed cover led to a drag reduction of 21 counts. Shortened boat tails also performed effectively in the studies outlined by [26] and [27], reporting drag reductions of 10.3% and 10.9% on a heavy and light-duty truck geometry respectively using wind tunnel tests. [28] reviewed various trailer-mounted aerodynamic devices for heavy trucks and recommended boat tail lengths between 24 and 32 inches for a viable trade-off between performance and practicality. The influence of specific panel configurations on rear cavities was explored in [29], which showed a full enclosure with tapering of 10 degrees maximised performance, and that removing lower panels significantly reduced the drag reduction. Overall, these studies highlight that significant drag and fuel savings are realisable through the integration of a rear tail or cavity device appended to the base of a road vehicle.

3 Road Testing Methodology

3.1 Measuring a Drag Change on-Road

The method described next for measuring a drag change on-road was first described in [30], therefore only a brief summary of the technique will be provided next. The method involves fixing the vehicle's throttle pedal across two vehicle configurations. For a given, fixed, throttle position, a road vehicle will reach a constant equilibrium speed for its configuration on a long flat straight road. This happens because by fixing the vehicle's throttle pedal, the fixed power output from the engine is used to counteract both the drag and the rolling resistance force on the vehicle. It was confirmed in [30] that fixing the vehicle's throttle pedal across configurations does produce a fixed power output from the engine, which was confirmed via three different power measurements remaining constant for multiple different configurations with two different vehicles. An example to demonstrate the method is as follows: The baseline standard vehicle has its throttle pedal fixed at 35% compression, the vehicle will then reach a constant speed on a long, flat, straight road, V_1. The vehicle is then configured in some way, such as by adding a kayak to its roof. When this configured vehicle travels down the same road with the same throttle pedal compression it will reach a new speed, V_2. The resulting speed delta measured on the road, V_1 - V_2, can then be used with the equation set discussed next to determine the percentage drag change on the vehicle.

3.1.1 Governing Equations

The derivation for the percentage drag change equation begins from the constant power statement (Equation 1), which becomes Equation 2, as the only two forces acting on a vehicle once it reaches its equilibrium speed for a given power input are drag and rolling resistance.

$$P_1 = P_2 \tag{1}$$

$$(D_1 + R_1)(V_1) = (D_2 + R_2)(V_2) \tag{2}$$

A reasonable assumption to apply is that the rolling resistance force between the two configurations at the speeds V_1 and V_2 remains constant. This is valid as the measured speed delta is often less than 10 km/h, and the rolling resistance force change across such a speed delta would be minimal [31]. Applying this assumption to Equation 2, the power balance then becomes Equation 3.

$$\frac{1}{2}\rho V_1^3 C_{D1} A_1 + RV_1 = \frac{1}{2}\rho V_2^3 C_{D2} A_2 + RV_2 \tag{3}$$

Equation 3 can then be rearranged to isolate the drag area of the vehicle in its second configuration, which can then be subbed into the percentage drag change formula to produce Equation 4. This is the final equation of the derivation, which is used to determine the percentage change in drag for a baseline vehicle caused by any given configuration change.

$$C_{D2}A_2 = \frac{\frac{1}{2}\rho V_1^3 C_{D1} A_1 + R(V_1 - V_2)}{\frac{1}{2}\rho V_2^3}$$

$$\%Drag\ Change = \frac{D_2 - D_1}{D_1} = \frac{C_{D2}A_2 - C_{D1}A_1}{C_{D1}A_1} = \frac{C_{D2}A_2}{C_{D1}A_1} - 1$$

$$\%Drag\ Change = \left(\left(\frac{V_1}{V_2}\right)^3 + \frac{2R(V_1 - V_2)}{\rho V_2^3 C_{D1}A_1} - 1\right) 100 \tag{4}$$

The percentage drag change determined by Equation 4 is primarily determined by the values inputted for the road-measured speeds, V_1, and V_2. To apply the formula, an approximate estimate of the baseline vehicle's drag area and rolling resistance is required. It was shown in [30] via a sensitivity analysis, that only general estimates of these values are required, as the formula is relatively insensitive to the values used for the drag area, $C_{D1}A_1$, and R. The formula's primary sensitivities are related to the values inputted for V_1 and V_2, highlighting the need for the accurate determination of the road-measured speeds using GPS to gain representative results.

3.1.2 Test Track & Testing Conditions

A 3.5 km section of public road was used as the test track which can be seen in Figure 1. The test track was comprised of a main test section and two pretest sections which led into the main test section from either side. To ensure minimal interference from external traffic, all road tests were conducted between the hours 1–4 am. The vehicle's throttle pedal was fixed at the start of the pretest section after which the vehicle begins to reach its equilibrium speed, which usually occurs just prior to entering the main test section. At the centre of the main test section, the vehicle's speed is recorded using dual frequency GPS, which has a speed measurement accuracy of 0.25 km/h based on the number of satellites the GPS can access along the test track. The vehicle's speed is recorded using several runs travelling in both directions. Testing was conducted only on dry calm nights, where the external wind speed was measured to be less than 2 km/h using a handheld hot wire anemometer at the centre of the test track over a period of 90 s. In general, the external wind speed for most test nights was less than 1 km/h, and any slight wind was accounted for by recording the vehicle's speed when coming from both directions. The track has substantial tree cover either side which added additional protection from any slight external wind which came perpendicular to the track. In general, the averaged speeds recorded when coming from both directions were approximately the same, or varied by at most 1-2 km/h due to any slight external wind conditions during testing. Any runs which encountered traffic interference that would have affected the equilibrium speed recorded at the speed record point were scrapped, however scrapping a run was uncommon due to the minimal traffic interference along the test track during the testing hours stated.

3.1.3 Testing Procedure & Test Vehicles

The throttle pedal position for the test vehicles was monitored using an OBD II Bluetooth scanner (OBDLink MX+). This scanner also provided information on the vehicle's power output based on measurements from quantities such as mass air flow rate and fuel injection data. As stated previously, the power output measured using three different power indicators during testing confirmed that the engine's power output remained constant across configuration changes for a fixed throttle pedal. Prior to any speeds being recorded, the test vehicle was warmed up for approximately 20–30 minutes by

Figure 1: Images of the test track with details of the main and pretest sections. Adapted from [30].

driving it along the test track. This allowed the vehicle's engine, tires and other moving components to reach normal operating temperatures. In general, a given vehicle configuration required 6–10 runs until the vehicle's constant equilibrium speed could be determined. This was done by observing a modal speed for the runs in each direction. Once the modal speed was recorded in each direction after the required number of runs, an average of these two speeds was taken, which resulted in the overall equilibrium speed recorded for a given vehicle configuration. The two test vehicles used for the study were a 2017 VW Golf Mk7 1.6 L diesel, and a 2018 Citroen Berlingo commercial van 1.6 L diesel L1 H1. Both these vehicles are shown in Figure 2.

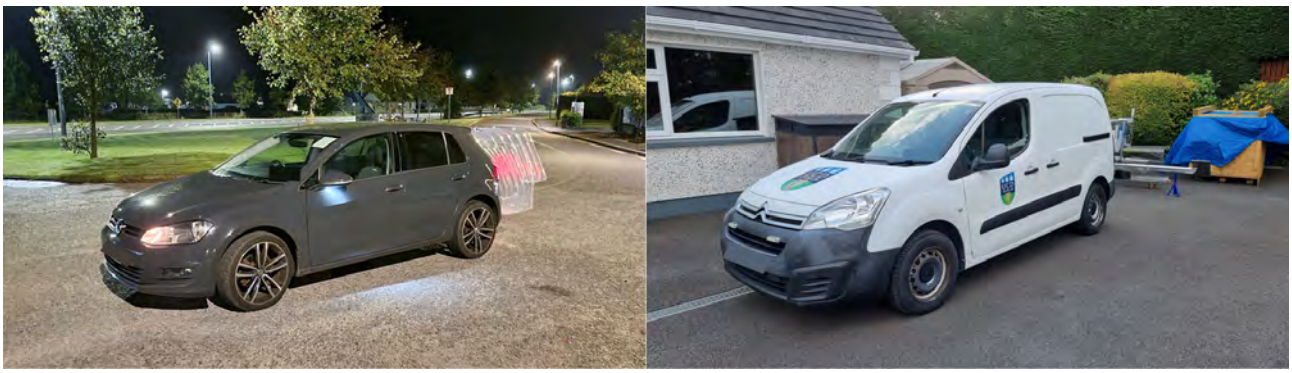

Figure 2: The two test vehicles used in the study which included a VW Golf Mk7 (shown left with an inflatable device) and a Citroen Berlingo L1 H1 van (right).

As stated previously, to use Equation 4 a rough estimate of the test vehicle's baseline drag area and rolling resistance were required. The VW Golf Mk7 was taken to have a C_D value of 0.305 based on CFD results [30] and outline values based on online sources where the manufacturer claims the vehicle to have a C_D value between 0.3 - 0.31 depending on spec [32] [33]. The rolling resistance value for the VW Golf Mk7 was taken as 150 N, which was based on its mass and the road surface of the test track. This value is typical for a hatchback vehicle of this size, based on an example in [6] which outlines a similar value for a Mercedes Benz B-Class. The drag coefficient for the van was based on an online source stating it to be 0.35 [34], and the rolling resistance value was taken as 200 N, which accounts

for the van's larger mass, and condition based on a service life as a commercial van with over 100,000 km travelled. These values match those used in [30] for the same vehicles. The VW Golf Mk7 was used for this study on account of its availability to the authors as a personal vehicle and the Citroen Berlingo van was provided by the University of the authors to assist with research activities. The frontal areas for the vehicles were measured using a CAD frontal area projection tool using highly detailed STL files for both vehicles. The frontal areas for the car and van were measured as 2.113 m^2 and 2.800 m^2 respectively.

To ensure a fair comparison of the drag force deltas between road measurements and CFD predictions, the denominators in the percentage drag change formulas for the CFD data use the same reference values as those used for the road data. This means that in the percentage drag change formula for the van and car, the deltas are always divided by 0.35 and 0.305, respectively, when the areas for the vehicle configurations remain constant. For both the car and van, the frontal projected areas remained constant across all rear drag reduction device configurations, including when no devices were fitted.

4 Results & Discussion

4.1 On-Road Drag Change Measurements

All CFD-predicted drag changes stated in this section are based on the RANS methodology disucssed in [1]. The air density used for the CFD simulations was 1.2215 kg/m^3. When calculating the road-measured drag change using Equation 4, the same density value was applied. Although the most appropriate value for ρ is that measured on the testing night when V_1 and V_2 are recorded, the formula is highly insensitive to ρ. Therefore, for simplicity and consistency across tests with slightly varying air densities, and for direct comparison with CFD, a single value of 1.2215 kg/m^3 was used. To demonstrate this insensitivity, if a value of 1.25 kg/m^3 were used for ρ when calculating the road-measured drag change in Table 1, the result would shift only from 13.52% to 13.48%, confirming the suitability of using a single air density value.

An important consideration when interpreting the CFD-predicted drag changes for the inflatable and foam cavity devices is that the simulations are based on idealised CAD geometries. In practice, discrepancies existed between the CAD models supplied to the manufacturer and the final manufactured devices. The degree of sealing between each device and the vehicle rear also has a significant impact on the drag reduction achieved, with tighter seals generally producing greater benefits. Accurately representing the exact level of sealing in CAD is difficult due to the shape uncertainties when working with such devices. Therefore, the CFD-predicted drag changes for the inflatable and foam devices should be viewed as idealised indicators for the performance achievable under optimal manufacturing and sealing conditions.

4.1.1 Van with Inflatable Triple Cavity

A rigid triple cavity device for the Citroen Berlingo van was first outlined in [30]. An inflatable version of this device was developed in an attempt to preserve similar performance, while offering the added benefits of reduced weight, lower cost, and easier storage. Figure 3 outlines the final manufactured version of this device. A key limitation of inflatable devices is that their section thickness must be significantly greater than that of rigid devices. By having a thickened section for the cavities, the rear projected surface area on the multi cavity device is increased, which can negatively affect the drag reduction, as those rear surfaces are subjected to pressures below ambient static pressure. This is especially the case for the outer and middle cavity, but less so for the inner cavity which can have a positive pressure exerted on its rear face as it makes contact with a downstream high-pressure bubble. Details on how a multi cavity device reduces drag using this downstream high-pressure bubble are outlined in detail in [12] and [30]. The contrast between the manufactured inflatable and the idealised inflatable is shown in Figure 4, where the idealised version is free from any rippled surfaces and, most importantly, the end of the outer cavity features a taper. This taper was omitted from the real inflatable by the manufacturer due to the difficulty of incorporating it into the inflatable design. This tapered surface is needed to help the device converge the wake and reduce drag. By not having the taper, the drag reduction realised by the manufactured device was always going to be less than that for the idealised version.

Figure 3: A collection of images highlighting the inflatable triple cavity device for the van. This figure demonstrates the inflation process, how it is protected from hot exhaust gases (with an image of the shield on the VW Golf Mk7 for a better visual), and how it looks on the road from an aerial view.

One other interesting feature outlined in Figure 3, is that the device uses a silver reflective heat shield on its underside in the vicinity of the vehicle's exhaust pipe. This triple cavity device was one of the first inflatable devices to be manufactured and road tested in this study. On the first attempt at road testing with this device, the device was punctured due to the heat from the exhaust gases after approximately 30 minutes of driving. Following this incident, all subsequent inflatable devices were fitted with a heat shield in this area. This heat shield solution was very effective at protecting the devices, as no future ruptures of any inflatables due to exhaust heat occurred. This device can be inflated in approximately 2 to 3 minutes using a high-power, high-flow-rate pump (shown in Figure 3). The device attaches to the vehicle via hooks that engage the panel gap between the doors and body, with straps linking the hooks to O-rings on the inflatable's surface. Brake lights, indicator signals, and the rear licence plate are still visible when the device is attached to the vehicle.

Configuration Name	V_1 (km/h)	V_2 (km/h)	Road-Measured $\Delta Drag$	CFD Predicted $\Delta Drag$
Van Inflatable Triple Cavity	99	103.25	-13.5%	-16.3%*

Table 1: Drag change results for the van with the inflatable triple cavity.
(*) CFD prediction based on idealised geometry for the device.

Table 1 outlines the drag reduction results for this device on the van. The road-measured drag reduction based on the road-measured speeds V_1 and V_2 was 13.5%. When driving on the road with

this inflatable device, the van is noticeably much quieter, as the level of turbulence in the van's wake is significantly reduced due to the presence of the device. It was also observed to handle better in corners, likely due to a more stable base wake in the slightly yawed flow encountered during cornering. The CFD predicted drag change using an idealised model for the device was found to be 16.3%. This was based on the delta between the CFD predicted C_D for the baseline van (0.297) and that for the inflatable device (0.240), divided by the road value for the van's C_D, 0.35, outlined previously in Section 3.1.3. To quantify the effect the level of sealing between the device and the vehicle has on the drag reduction, an additional CFD simulation was performed. This showed that if the device was perfectly sealed against the van, the C_D value for the device drops to 0.228, producing a drag reduction of 19.7%. This highlights the need for caution when comparing road-measured results with CFD predictions for flexible or slightly deformable devices.

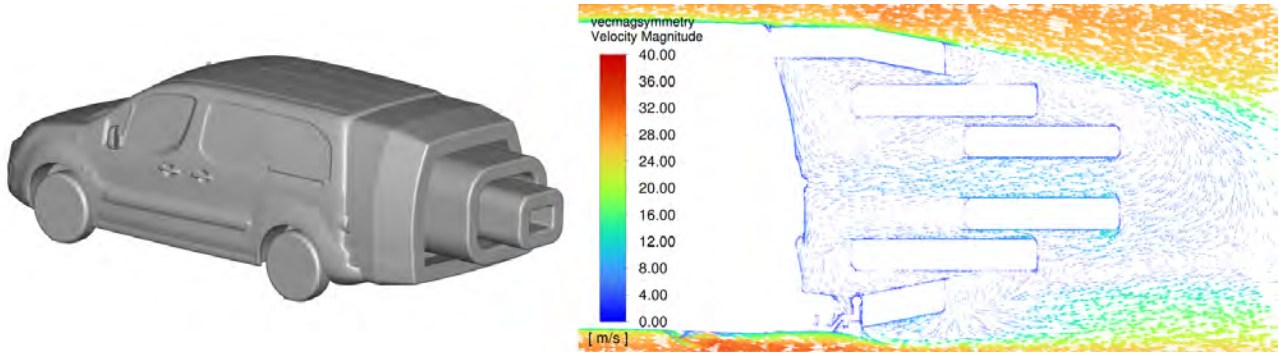

Figure 4: Outline of the CFD model and idealised shaped for the van's inflatable triple cavity (left) with the velocity flow field inside the device along the vehicle's symmetry plane (right).

4.1.2 Van with Inflatable Single Cavity

Having demonstrated that an inflatable triple cavity device could be constructed, a single cavity device was developed to offer similar performance. This was achieved mainly by changing the shape of the bottom section, removing the taper and raising it slightly from the bottom trailing edge of the van. This change was made because the bottom taper on the triple cavity device did not have attached flow, and it reduced performance by increasing the rear projected surface area exposed to underpressured flow. Additionally, removing the inner two cavities reduced the rear projected area, which helped further increase drag reduction, as the device now carried less self drag. Figure 5 outlines the manufactured inflatable single cavity, while Table 2 details the road-measured and CFD predicted drag reductions. It is notable that the CFD predicted drag reduction for the single cavity (-18.0%) is greater than that for the triple cavity (-16.3%), this is mainly due to the single cavity's improved outer cavity design. If another inner cavity were designed to go inside this single cavity, the drag reduction would further improve, however, the improvement would not be as substantial as that seen when working with rigid thin section cavities. Therefore, because of the added self drag associated with the thicker sections of inflatable devices, implementing them as single cavities is generally more practical, as the marginal gains from using multiple cavities are not large enough to justify the extra material and size.

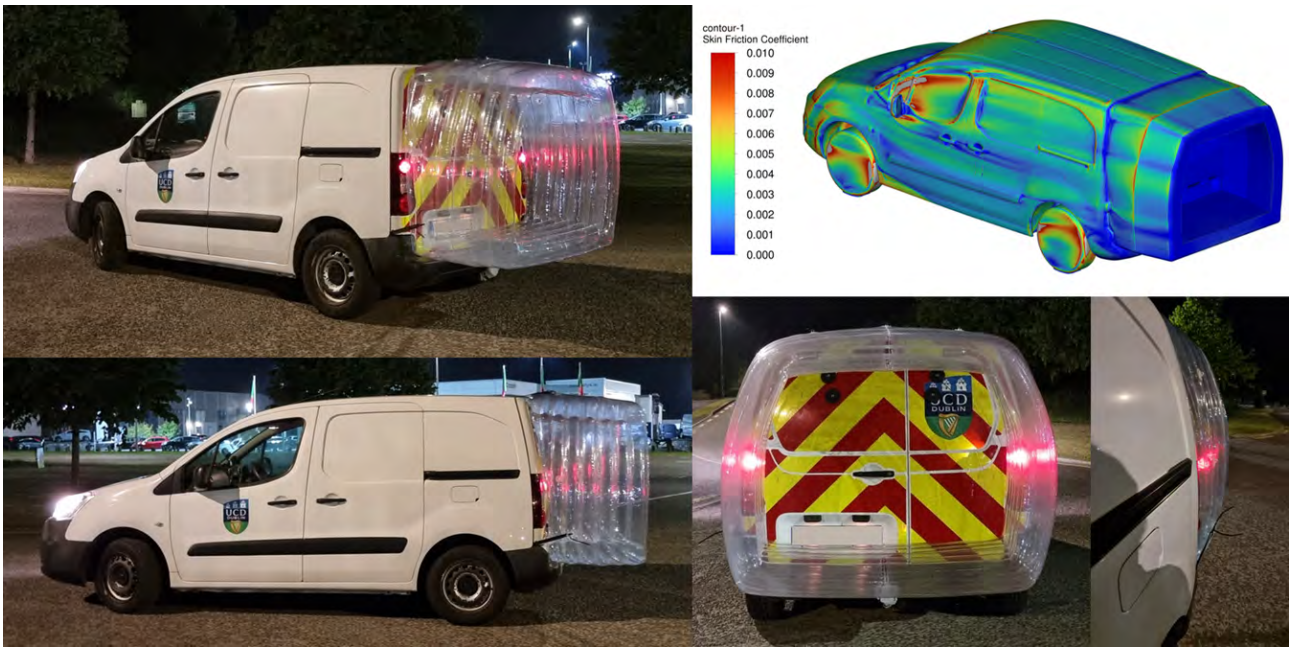

Figure 5: Images highlighting the inflatable single cavity device on the van. Shown top right is a skin friction coefficient contour plot along the configuration's surface.

The road-measured speed, V_1, for the unconfigured van outlined in Table 2, is notably much higher than that detailed in Table 1. This was because the road testing associated with the triple cavity device was performed with 35% throttle compression across configurations, while 37% was used for the single cavity device. The 35% throttle compression was chosen for the triple cavity testing in order to keep the recorded road speeds closer to 100 km/h, as it was expected that the V_2 for the triple cavity device would be quite large if testing was performed at 37% throttle compression. The road-measured drag reduction for the inflatable single cavity device (-9.0%) was notably much lower than that predicted by the CFD (-18.0%) for an idealised device. The cause of the deviation was primarily due to the sizing of the manufactured device, which was slightly too large for the base of the vehicle. This over-sizing issue can be observed in Figure 5, where the top and sides of the inflatable slightly protrude out past the base of the van into the flow. Additionally, the stated CFD predicted value is based on a tightly sealed inflatable against the rear of the van. This level of sealing was not present on the real device, particularly on the side sections near the van's lights. Another major cause of the discrepancy is the shape deviations, particularly the rippled surface and the general absence of tapering on the top and sides, which differ significantly from the idealised device.

Configuration Name	V_1 (km/h)	V_2 (km/h)	Road-Measured $\Delta Drag$	CFD Predicted $\Delta Drag$
Van with Inflatable Single Cavity	106.75	109.75	-9.0%	-18.0%*

Table 2: Drag change results for the van with the inflatable single cavity.
(*) CFD prediction based on idealised geometry for the device.

4.1.3 Car with Foam Cavity

One of the main disadvantages of inflatable devices is the difficulty in making their shape match the desired form drawn and studied in CAD and CFD. A solution to this was to construct a single cavity device from foam for the VW Golf, CNC milled to allow a closer match between the CAD geometry and the real device. The foam device shown in Figure 6 was constructed from EPS foam, wrapped in aluminium tape, and coated in polyurea paint to provide added strength, waterproofing and general weather resistance. The final device was a very close match with the CFD model in terms of its overall shape. The CFD model for this device predicted a drag reduction of 27.5% as detailed in Table 3. This idealised reduction is based on a perfect seal between the device and the rear of the car, combined with perfect alignment of the device. The main discrepancies between the real device and the CFD model were related to a reduced level of sealing, and the alignment of the device. On the night when this device was road tested, the device was slightly misaligned, such that the device was tilted backwards slightly. This can be partially seen in the top left image of Figure 6. This was only observed when reviewing the images of the road tested device after the testing and comparing them with how the CFD model had the device aligned.

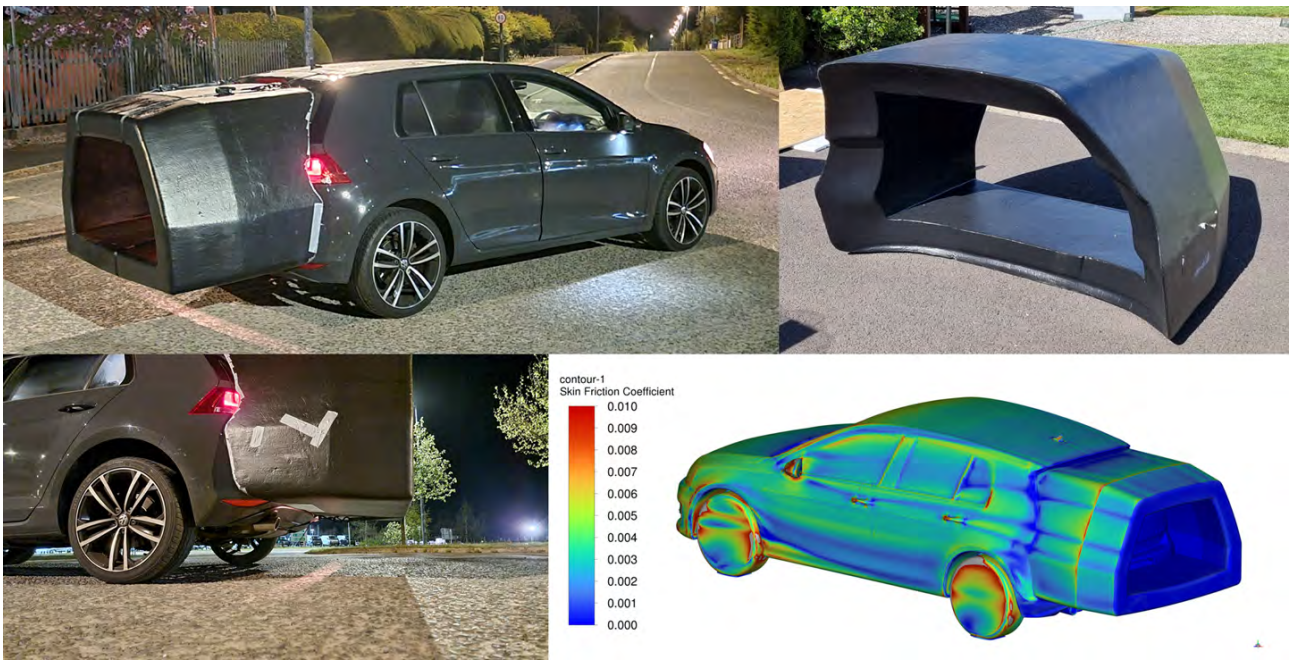

Figure 6: Images highlighting the foam single cavity device for the car with a skin friction coefficient contour plot along the configuration's surface shown bottom right.

Even with these deviations, the road-tested device still achieved an appreciable 17.4% drag reduction. If the device were better sealed and correctly aligned it would be very likely to produce a drag reduction in excess of 20%. Driving with this device on the VW Golf had a very noticeable effect on its speed and acceleration, with the car reaching highway speeds with substantially less throttle effort. The device was light enough to be installed on the vehicle by a single individual. Additionally, when viewed from the rear, both the licence plate and rear lighting systems were visible with only minor obstruction.

This device could be further refined by reducing its section thickness, taking its current size down from approximately 150 mm to 75 mm. This would improve both rear visibility and the realised drag reduction, as reducing the rear projected surface would lower the self drag on the cavity's rear face.

Configuration Name	V_1 (km/h)	V_2 (km/h)	Road-Measured $\Delta Drag$	CFD Predicted $\Delta Drag$
Car with Foam Cavity	99	104.5	-17.4%	-27.5%*

Table 3: Drag change results for the car with the foam cavity.
(*) CFD prediction based on idealised geometry for the device.

4.1.4 Car with Inflatable Double Cavity

As the rear of the VW Golf was smaller than that of the Citroen Berlingo van, constructing a triple cavity inflatable device for it was not feasible given the required section thickness for each cavity when made from inflatable material. Therefore, to demonstrate a multi cavity inflatable device on the passenger car, a double cavity variant was designed and manufactured, as shown in Figure 7. This device was made primarily to study its usability instead of pursuing a maximum drag reduction. This was due to the van inflatable device results, which indicated that when manufacturing rear devices from inflatable material, the gains from using multi cavity variants are only marginal due to manufacturable shape constraints. A major issue with this device was the lack of support for the inner cavity when connected to the outer cavity. To help support it, a cable tie chain was used to connect the ends of the top surfaces of the outer and inner cavity, which can be seen in the images of Figure 7. Even with this support, the inner cavity was observed to bounce/oscillate slightly in the vertical direction when on the road during testing.

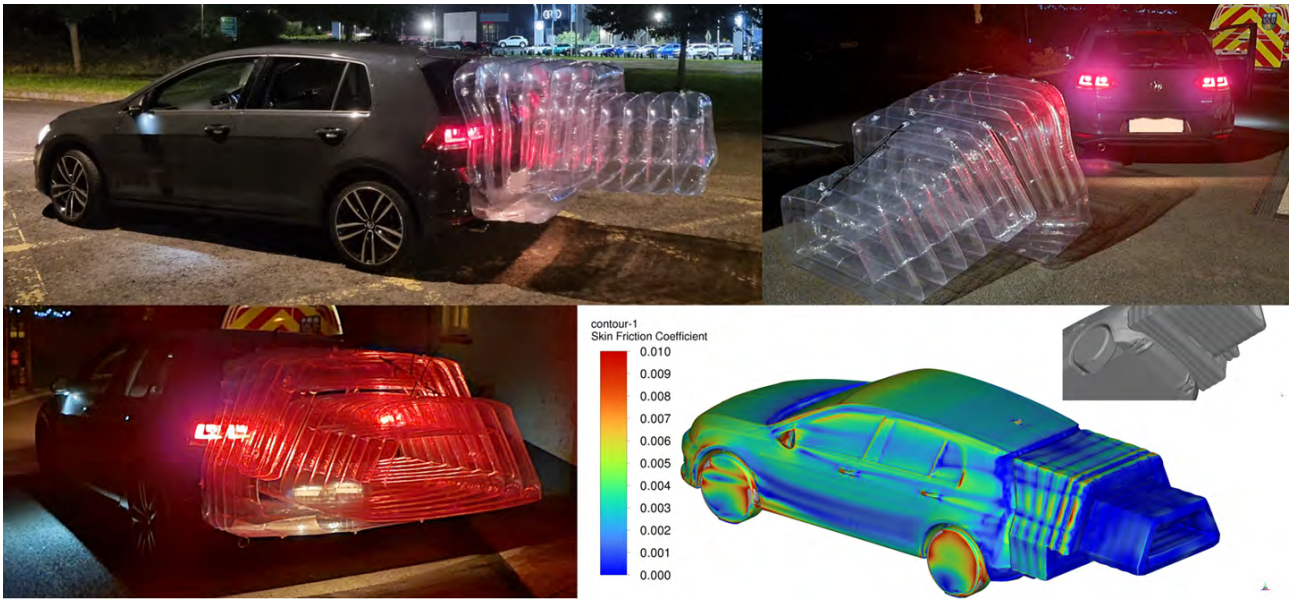

Figure 7: Images highlighting the inflatable double cavity device for the car with a skin friction coefficient contour plot along the configuration's surface shown bottom right.

Therefore, the road-measured drag reduction presented in Table 4 was always unlikely to match that predicted with the CFD model. The bouncing issue combined with a general lack of sealing between the device and the lower rear of the VW Golf is primarily what caused the road-measured reduction to realise just 8% compared to the 16.4% predicted with CFD. Figure 7 includes an image showing the level of sealing between the underside of the device and the car for the CFD model, which was tightly sealed. This contrasted with the manufactured device, which had a noticeable gap in this region.

Configuration Name	V_1 (km/h)	V_2 (km/h)	Road-Measured $\Delta Drag$	CFD Predicted $\Delta Drag$
Car with Inflatable Double Cavity	102.5	105	-8.0%	-16.4%*

Table 4: Drag change results for the car with the inflatable double cavity.
(*) CFD prediction based on idealised geometry for the device.

4.1.5 Car with Adapted Inflatable Double Cavity

Given that the inner cavity of the car's inflatable double cavity was prone to bouncing, an adapted version was created by cutting it away. This effectively made a single cavity device for the car using just the outer section of the original double cavity. Figure 8 shows this device, while Table 5 presents its road-measured results. Removing the inner cavity did reduce the device's performance, demonstrating just a 5% drag reduction for its adapted single cavity variant in comparison to its original 8% drag reduction as a double cavity. While the realised drag reduction was smaller, the adapted version of this device was significantly more practical and user-friendly. This is shown in the lower images of Figure 8, which illustrate how the device can be easily manoeuvred to allow access to the vehicle's rear storage space.

Figure 8: Images highlighting the adapted (inner-removed) inflatable double cavity device for the VW Golf. Shown is an outline for how the inner cavity was cut away and how the device can be manoeuvred to facilitate access to the rear boot space and how it can be easily deflated and stored.

Reaching through the centre of the device to open the boot was made easier with the inner cavity removed. Additionally, the device can be easily flipped onto the roof of the car to access the boot, or it can remain attached to the hatch as the boot opens. Another benefit of this smaller device is that it can be quickly deflated and easily stored in the boot, taking up less space as a result of the reduced material. The original double cavity can be stored and manoeuvred in a similar way, but it requires more effort and must be fully deflated to fit in the boot, whereas the single variant requires only partial deflation.

Configuration Name	V_1 (km/h)	V_2 (km/h)	Road-Measured $\Delta Drag$
Car with Adapted Inflatable Double Cavity	102	103.5	-5.0%

Table 5: Drag change results for the car with the adapted (inner-removed) inflatable double cavity.

4.2 Surface Pressure Measurements

4.2.1 Van with Rigid Triple Cavity

The inflatable triple cavity device for the Citroen Berlingo van previously detailed in Section 4.1.1 was based on a rigid triple cavity device which was first studied in [30]. This rigid device (shown in Figure 9) was used in this present study to quantify the changes to the van's base pressure map once the device was fitted. Six base pressure patches, labelled A–F, were fitted to the van's rear, which was divided horizontally into three sections, with patches A–B, C–D, and E–F representing the top, middle, and lower sections, respectively. Table 6 outlines the recorded pressure deltas on each of the six patches for the three measurement methods. The road-measured pressure deltas show that the largest base pressure increase occurred on the lower section of the van once the device was fitted, with patches E and F reporting increases of 64 Pa and 75 Pa respectively. The next largest pressure increase was recorded on the middle section, with the top section showing the lowest pressure rise.

Figure 9: Images showing the locations of the six base pressure patches fitted to the Citroen Berlingo van (left) and the rigid triple cavity device fitted to the van for testing (right).

Patch Pressure Difference ΔP (Pa)	A	B	C	D	E	F
Road-Measured	24	20	34	52	64	75
RANS	58	63	52	91	36	49
HLES	23	32	30	46	69	87
RANS Error	34	43	18	39	-28	-26
HLES Error	-1	12	-4	-6	5	12

Table 6: Pressure deltas recorded at each of the six patches shown in Figure 9 using the three different measurement methods, with an outline for the errors between the CFD methods and the experiment.

The HLES method successfully predicted this trend with relatively high accuracy, with four out of the six patches demonstrating an error of 6 Pa or less. In contrast, the RANS methodology predicted a noticeably different change to the van's base pressure map, predicting a greater pressure increase in the upper section compared to the lower section. The limitations of RANS in accurately predicting base pressure distributions for squareback geometries are well documented in the literature. Notably, the AutoCFD workshops [35] [36] provide a relevant example, where simulations on a squareback Windsor body using RANS models showed significant discrepancies compared to experimental results, whereas scale-resolving methods demonstrated improved agreement. While RANS struggles to predict the exact shape change to the base pressure map as a result of the rear device, it remains valuable in predicting overall changes in C_D during development. For this device, the RANS method predicted a total drag reduction of 65 counts once fitted to the van, while the HLES method predicted a slightly higher 76 counts.

[30] demonstrated that predictions of drag force changes using RANS showed a high level of agreement with on-road measurements when appendable devices were fitted to road vehicles. For example, the road-measured drag reduction for this device on the van reported in [30] was 17.5%, which correlated closely with the 18.6% reduction predicted using RANS. In contrast, the HLES method would have predicted a notably higher reduction. When working with CAD models of vehicles that have smooth undersides and no internal flows, RANS can produce results that more closely match road measurements due to a potential beneficial cancellation of errors. A rear drag reduction device is likely to produce a greater drag reduction when fitted to a vehicle with a smooth underside, as the lower turbulence and improved flow attachment in the underside flow interact more effectively with the device, leading to enhanced downstream pressure recovery and increased base pressure. Vehicles with messy undersides will experience the opposite effect, reducing the effectiveness of the device. Therefore, the lower drag reductions predicted using RANS are more likely to align with on-road measurements due to a beneficial cancellation of errors when simulating such CAD geometries.

4.2.2 Car with Foam Cavity

The foam cavity device fitted to the VW Golf Mk7, outlined in Section 4.1.3, was equipped with six base pressure patches, as shown in Figure 10. This was done to correlate the road-measured drag reduction of 17.4% with a corresponding average base pressure increase resulting from the device. Due to the difficulty in CAD modelling the exact level of sealing between the car and the device, no comparisons are made to the CFD pressure changes, as the CFD base pressure measurements are highly sensitive to the represented/modelled level of sealing between the device and the car. Table 7 outlines the road-measured patch pressures for each of the six patches for both vehicle configurations. The rear of the car experiences a substantial base pressure increase with the device, as it taps into a higher downstream pressure and distributes this over its base. The cavity, particularly with its end tapers, enhances downstream static pressure recovery, benefiting the overall base pressure increase on the car's rear. The top (A-B) and middle (C-D) sections experienced the largest pressure increase, with reported deltas of approximately 50 Pa over both sections.

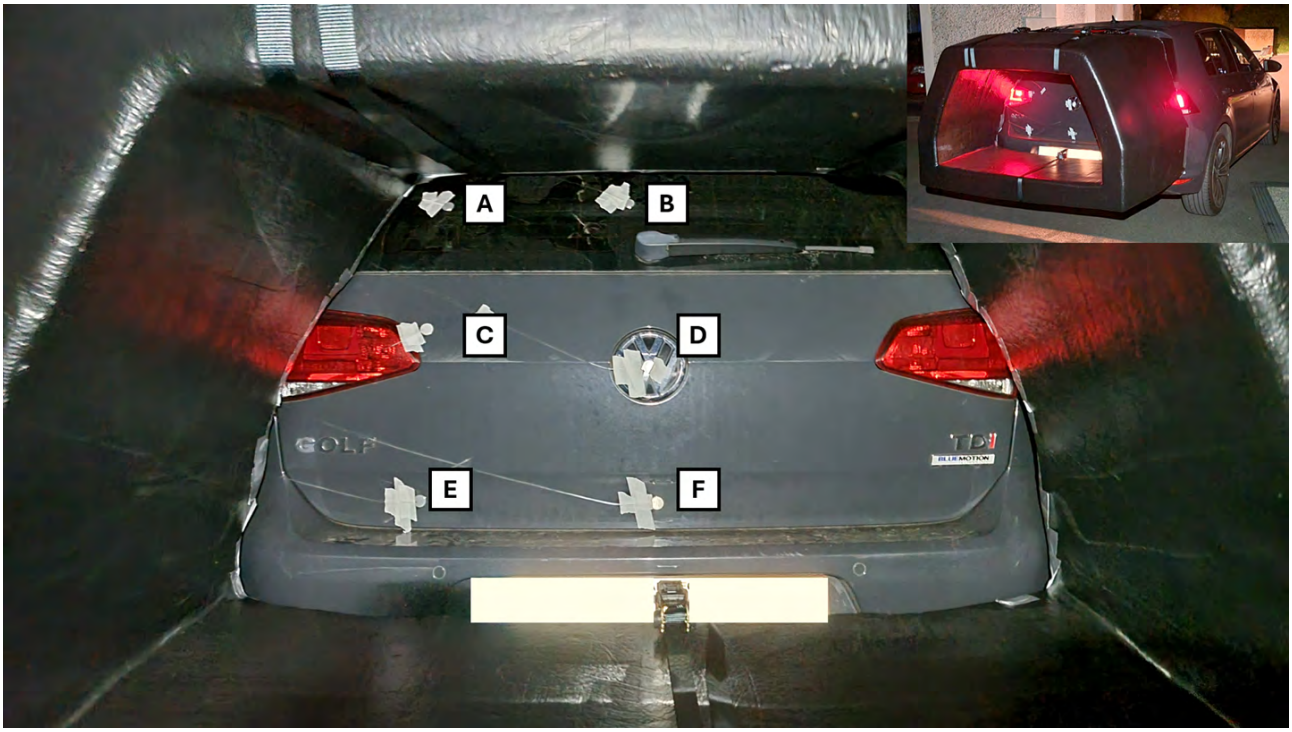

Figure 10: Locations of the six base pressure patches fitted to the VW Golf Mk7 during the surface pressure testing with the foam cavity device.

Based on the percentage base pressure increases for the six patches in Table 7, the overall average base pressure rise for the rear is likely between 40% and 50% as a result of the device. A CFD analysis of the baseline car revealed that approximately 50% of the total drag force is carried by the rear alone. For the real vehicle, this value is likely slightly less when accounting for the vehicle's internal flows, detailed wheels, and less smooth underside. Therefore, the true portion of the total drag force carried by the VW Golf's rear is likely between 40-50%. Taking this as 45% for the purpose of applying a

weighting to the measured base pressure increase of 40-50%, the estimated drag reduction for this base pressure rise is likely between 18% and 22.5%. This estimate does not account for the additional self drag present on the foam cavity, particularly on its angled tapers and end faces, due to their rear-projected surfaces. When accounting for this, the drag reduction is likely closer to the 18% estimate rather than the higher value of 22.5%. Therefore, the road-measured drag reduction of 17.4% shows reasonably good agreement with the estimated drag reduction, based on the measured base pressure increases.

Road-Measured Patch Pressure (Pa)	A	B	C	D	E	F
VW Golf Mk7	-107	-110	-114	-111	-100	-94
VW Golf Mk7 with Foam Cavity	-59	-58	-58	-63	-58	-61
Delta	48	52	56	48	42	33
|% Base Pressure Increase|	45%	47%	49%	43%	42%	35%

Table 7: Pressure measurements from each of the six pressure patches (as shown in Figure 10) for the VW Golf Mk7, with and without the foam cavity.

4.3 Surface Flow Measurements - Car with Taxi Sign

As outlined by the surface flow measurement methodology detailed in [1], averaged images of tufts produced from video-recorded imagery provide a better understanding of surface flow in transient regions compared to reviewing instantaneous single images. The wake of the taxi sign is one such region, where instantaneous images reveal little about the overall surface flow behind the sign. Figure 11 presents an averaged image of the surface flow in the wake of the taxi sign, alongside CFD predictions of the same flow. Four distinct regions, labelled 1–4, are identifiable in the averaged image and show good agreement with the CFD. Region 1 highlights how the flow begins to wrap inwards far downstream in the wake of the taxi sign. Region 2 illustrates how some of the flow is able to pass beneath the centre of the taxi sign at high speed, which is captured by the very straight alignment of the tufts in the top image of Figure 11. This compares well with the lower CFD skin friction plot, where a green/orange-coloured zone is clearly identifiable in this region, highlighting this fast-moving, attached flow.

Region 3 is identified as the end of a recirculation bubble directly behind the taxi sign along the vehicle's centreline, indicated by the vertical standing tufts. Identifying Region 3 using only instantaneous images was difficult and generally inconclusive. In contrast, the averaged image clearly reveals its presence. The CFD predicts this feature effectively, as shown by the vector plot along the symmetry plane in the lower image of Figure 11. Finally, Region 4 shows a zone of reversed flow in the wake of the taxi sign, extending along the centre of the roof noticeably far downstream. This extensive reversed flow region is also visible in the CFD vector plot, which indicates a similar downstream extent. Overall, Figure 11 demonstrates the usefulness of averaged tuft imagery in understanding overall surface flow patterns in highly transient regions, providing a reliable basis for meaningful, validatable comparisons against CFD-predicted surface flow behaviour.

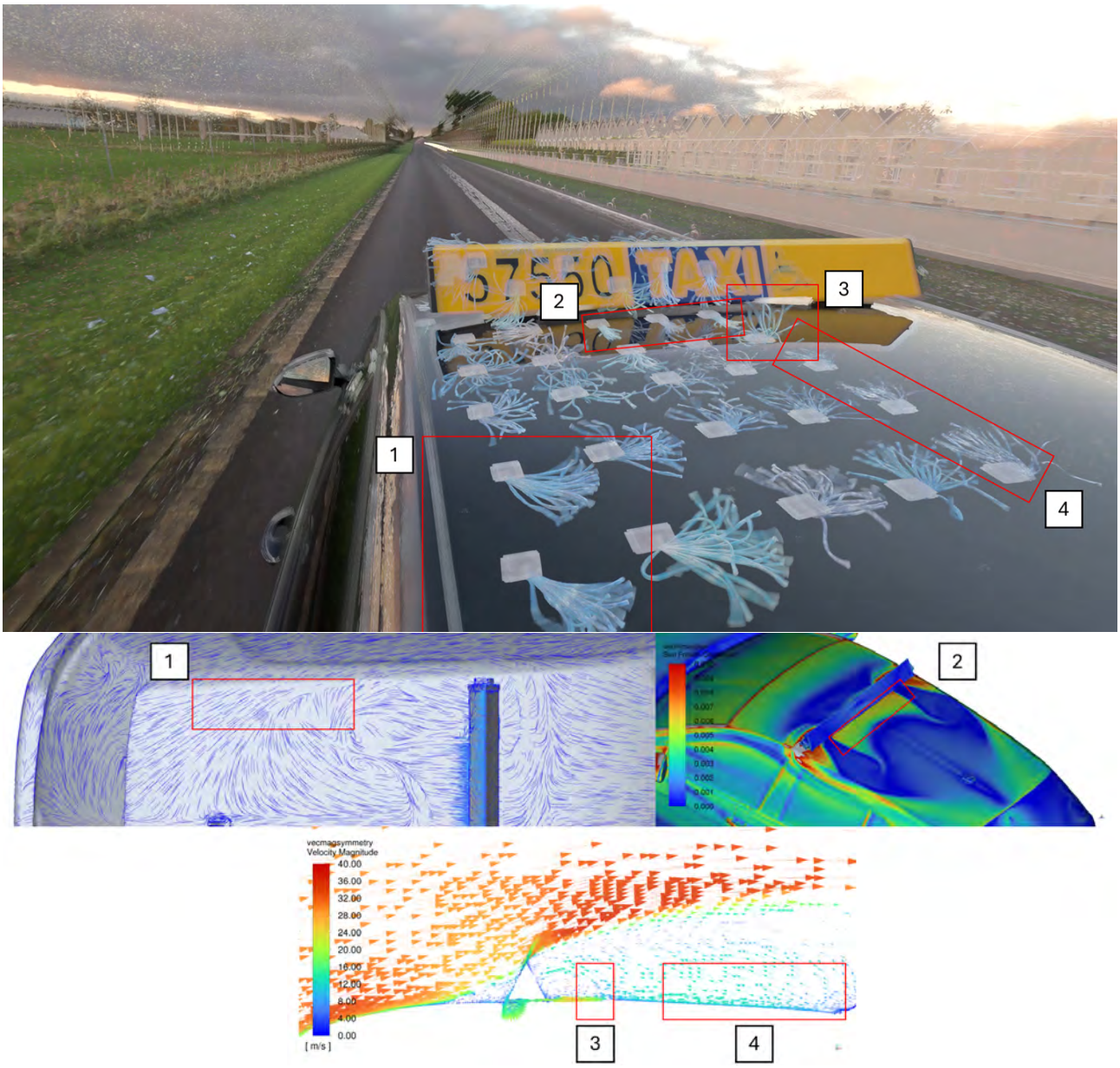

Figure 11: Comparison between the road-measured surface flow and that predicted using CFD for the VW Golf Mk7 fitted with the Irish taxi sign.

5 Conclusions

- A detailed look at some of the latest developments in appendable drag reduction technology for road vehicles was outlined, presenting results on inflatable rear cavity devices, one foam device, and a rigid triple-cavity device. Of the inflatable devices presented, these include findings for single, double, and triple cavity variants. These devices were road tested and simulated using CFD on two road vehicles: a VW Golf Mk7 and a Citroen Berlingo van.

- The best-performing road-tested inflatable device was a triple cavity mounted to the van, which reduced drag by 13.5%. Overall, inflatable devices were found to have practical benefits over rigid devices, such as easier storage and mounting. However, their drag reduction performance was closely linked to their manufactured shape and the level of sealing between the inflatable and the rear of the vehicle. Producing an inflatable device that matches the CAD model used in the CFD studies during development can be difficult, and performance degradation was observed due to shape deviations such as rippled surfaces, thickened sections, lack of tapering, and incomplete sealing with the vehicle.

- Due to the thickened section required when working with inflatable devices, an additional self drag penalty is incurred, as the increase in rear-projected surface area results in an added rearward drag force. This contrasts with thin-section rigid devices, where a panel can have near-negligible self drag. This led to the conclusion that implementing inflatable devices as multi cavity variants offers only marginal benefits, as the added drag reduction can be offset by the increased self drag from the thicker cavity sections.

- The observed driving properties of the test vehicles when fitted with a rear drag reduction device were noticeably improved over the standard vehicles. Clear increases in acceleration, reduced throttle effort for maintaining road speeds, and improved handling while cornering were all observed when driving with some of the most effective rear devices outlined in this article.

- Road testing with a foam cavity device mounted to the VW Golf Mk7 was found to reduce drag by nearly 20%, with corresponding base pressure measurements indicating the device offered a near 50% increase in base pressure inside the cavity. Additionally, base pressure measurements taken from a van fitted with a rigid triple cavity device also showed substantial base pressure increases. When compared with CFD, scale-resolving methods such as Hybrid-LES were found to offer much closer agreement with the road-measured pressure deltas than the RANS methods, even though both CFD approaches predicted similar overall drag deltas for the device.

Funding

This research was funded by The Irish Research Council grant number EPSPG/2022/213 and Science Foundation Ireland grant number 22/NCF/EI/11277.

Acknowledgments

The support of UCD SONIC and ICHEC for the use of their HPC resources.

References

[1] Michael Gerard Connolly, Alojz Ivankovic, and Malachy J. O'Rourke. Developments in Drag Reduction Methods and Devices for Road Vehicles. *Applied Sciences*, 15(17):9693, January 2025. ISSN 2076-3417. doi: 10.3390/app15179693. URL https://www.mdpi.com/2076-3417/15/17/9693. Publisher: Multidisciplinary Digital Publishing Institute.

[2] Noraini Zulkifli and Daniel Haqeem. The Opec Oil Shock Crisis (1973): An Analysis. *Asian Journal of Research in Business Economics and Management*, 4:136–148, March 2022. doi: 10.55057/ajrbm.2022.4.1.12.

[3] David Banister. The climate crisis and transport. *Transport Reviews*, 39(5):565–568, September 2019. ISSN 0144-1647. doi: 10.1080/01441647.2019.1637113. URL https://doi.org/10.1080/01441647.2019.1637113. Publisher: Routledge _eprint: https://doi.org/10.1080/01441647.2019.1637113.

[4] Sudarshan Gnanavendan, Senthil Kumaran Selvaraj, S. Jithin Dev, Kishore Kumar Mahato, R. Srii Swathish, G. Sundaramali, Oussama Accouche, and Marc Azab. Challenges, Solutions and Future Trends in EV-Technology: A Review. *IEEE Access*, 12:17242–17260, 2024. ISSN 2169-3536. doi: 10.1109/ACCESS.2024.3353378. URL https://ieeexplore.ieee.org/document/10398193.

[5] Caroline Kuzemko, Mathieu Blondeel, Michael Bradshaw, Gavin Bridge, Erika Faigen, and Louis Fletcher. Rethinking Energy Geopolitics: Towards a Geopolitical Economy of Global Energy Transformation. *Geopolitics*, 30 (2):531–565, March 2025. ISSN 1465-0045. doi: 10.1080/14650045.2024.2351075. URL https://doi.org/10.1080/14650045.2024.2351075. Publisher: Routledge _eprint: https://doi.org/10.1080/14650045.2024.2351075.

[6] Thomas Christian Schuetz. *Aerodynamics of road vehicles*. Sae International, 2015. ISBN 0-7680-8253-6.

[7] Chun Li, Fan Yang, and Zhenchong Wang. Experimental study on high-speed endurance of electric vehicle at normal temperature (25℃). volume 268, page 01032. EDP Sciences, 2021. ISBN 2267-1242.

[8] Transport Canada. Review of Aerodynamic Drag Reduction Devices for Heavy Trucks and Buses, May 2018. URL https://tc.canada.ca/en/programs/non-funding-programs/ecotechnology-vehicles-program/review-aerodynamic-drag-reduction-devices-heavy-trucks-buses. Publisher: AHEC.

[9] The Effect of Aerodynamic Drag on Fuel Economy | ARC, . URL https://www.arcindy.com//effect-of-aerodynamic-drag-on-fuel-economy.html.

[10] K. Chow. Improving vehicle rolling resistance and aerodynamics. In Richard Folkson and Steve Sapsford, editors, *Alternative Fuels and Advanced Vehicle Technologies for Improved Environmental Performance (Second Edition)*, Woodhead Publishing Series in Energy, pages 459–481. Woodhead Publishing, January 2022. ISBN 978-0-323-90979-2. doi: 10.1016/B978-0-323-90979-2.00009-3. URL https://www.sciencedirect.com/science/article/pii/B9780323909792000093.

[11] Hyeonjik Lee and Kihyung Lee. Comparative Evaluation of the Effect of Vehicle Parameters on Fuel Consumption under NEDC and WLTP. *Energies*, 13(16):4245, January 2020. ISSN 1996-1073. doi: 10.3390/en13164245. URL https://www.mdpi.com/1996-1073/13/16/4245. Number: 16 Publisher: Multidisciplinary Digital Publishing Institute.

[12] Michael Gerard Connolly, Malachy J. O'Rourke, and Alojz Ivankovic. Reducing Aerodynamic Drag on Flatbed Trailers for Passenger Vehicles Using Novel Appendable Devices. *Fluids*, 8(11):289, November 2023. ISSN 2311-5521. doi: 10.3390/fluids8110289. URL https://www.mdpi.com/2311-5521/8/11/289. Number: 11 Publisher: Multidisciplinary Digital Publishing Institute.

[13] Michael Gerard Connolly, Alojz Ivankovic, and Malachy J. O'Rourke. Drag reduction technology and devices for road vehicles - A comprehensive review. *Heliyon*, 10(13):e33757, July 2024. ISSN 2405-8440. doi: 10.1016/j.heliyon.2024.e33757. URL https://www.sciencedirect.com/science/article/pii/S2405844024097883.

[14] Alberto Morelli. A New Aerodynamic Approach to Advanced Automobile Basic Shapes. SAE Technical Paper 2000-01-0491, SAE International, Warrendale, PA, March 2000. URL https://www.sae.org/publications/technical-papers/content/2000-01-0491/. ISSN: 0148-7191, 2688-3627.

[15] Magnus Urquhart and Simone Sebben. Optimisation of Trailing Edge Flaps on the Base Cavity of a Vehicle for Improved Performance at Yaw. *Flow, Turbulence and Combustion*, 109(2):309–326, August 2022. ISSN 1573-1987. doi: 10.1007/s10494-022-00323-z. URL https://doi.org/10.1007/s10494-022-00323-z.

[16] Kathleen M. McNamara, Jamey D. Jacob, Ben Loh, Ryohei Tsuruta, Taro Tsukada, Eiji Itakura, and Umesh Gandhi. Experimental Investigation of Drag Reduction on Automobiles With an Inflatable Boat-Tail. In *2018 Applied Aerodynamics Conference*, AIAA AVIATION Forum. American Institute of Aeronautics and Astronautics, June 2018. doi: 10.2514/6.2018-3964. URL https://arc.aiaa.org/doi/10.2514/6.2018-3964.

[17] Alessandro Capone and Giovanni Paolo Romano. Investigation on the effect of horizontal and vertical deflectors on the near-wake of a square-back car model. *Journal of Wind Engineering and Industrial Aerodynamics*, 185: 57–64, February 2019. ISSN 0167-6105. doi: 10.1016/j.jweia.2018.12.011. URL https://www.sciencedirect.com/science/article/pii/S0167610518306445.

[18] Magnus Urquhart, Max Varney, Simone Sebben, and Martin Passmore. Drag reduction mechanisms on a generic square-back vehicle using an optimised yaw-insensitive base cavity. *Experiments in Fluids*, 62(12):241, November 2021. ISSN 1432-1114. doi: 10.1007/s00348-021-03334-0. URL https://doi.org/10.1007/s00348-021-03334-0.

[19] Jeff Howell, Max Varney, Martin Passmore, and Daniel Butcher. The Aerodynamic Effects of a 3D Streamlined Tail on the Windsor Body. *Fluids*, 8(2):59, February 2023. ISSN 2311-5521. doi: 10.3390/fluids8020059. URL https://www.mdpi.com/2311-5521/8/2/59. Number: 2 Publisher: Multidisciplinary Digital Publishing Institute.

[20] R. L. Peterson. *Drag Reduction Obtained by the Addition of a Boattail to a Box Shaped Vehicle*. PhD thesis, August 1981. URL https://ntrs.nasa.gov/citations/19810020556. NTRS Author Affiliations: California Polytechnic State Univ. NTRS Report/Patent Number: NASA-CR-163113 NTRS Document ID: 19810020556 NTRS Research Center: Legacy CDMS (CDMS).

[21] Y. A. Irving Brown, S. Windsor, and A. P. Gaylard. The Effect of Base Bleed and Rear Cavities on the Drag of an SUV. SAE Technical Paper 2010-01-0512, SAE International, Warrendale, PA, April 2010. URL https://www.sae.org/publications/technical-papers/content/2010-01-0512/. ISSN: 0148-7191, 2688-3627.

[22] Eui Jae Lee and Sang Joon Lee. Drag reduction of a heavy vehicle using a modified boat tail with lower inclined air deflector. *Journal of Visualization*, 20(4):743–752, November 2017. ISSN 1875-8975. doi: 10.1007/s12650-017-0426-6. URL https://doi.org/10.1007/s12650-017-0426-6.

[23] Joshua P. Kehs, Kenneth D. Visser, Jeff Grossman, Jared Niemiec, Andrew Smith, and Charles M. Horrell. A Comparison of Full Scale Aft Cavity Drag Reduction Concepts With Equivalent Wind Tunnel Test Results. *SAE International Journal of Commercial Vehicles*, 6(2):486–497, September 2013. ISSN 1946-391X, 1946-3928. doi: 10.4271/2013-01-2429. URL https://www.sae.org/publications/technical-papers/content/2013-01-2429/. Number: 2013-01-2429.

[24] J Kehs, K Visser, J Grossmann, C Horrell, and A Smith. Experimental and full scale investigation of base cavity drag reduction devices for use on ground transport vehicles. pages 269–283. Springer, 2010.

[25] Kuo-Huey Chen and Bahram Khalighi. A CFD Study of Drag Reduction Devices for a Full Size Production Pickup Truck. SAE Technical Paper 2015-01-1541, SAE International, Warrendale, PA, April 2015. URL https://www.sae.org/publications/technical-papers/content/2015-01-1541/. ISSN: 0148-7191, 2688-3627.

[26] Drew Landman, Richard Wood, Whitney Seay, and John Bledsoe. Understanding Practical Limits to Heavy Truck Drag Reduction. *SAE International Journal of Commercial Vehicles*, 2(2):183–190, October 2009. ISSN 1946-391X, 1946-3928. doi: 10.4271/2009-01-2890. URL https://www.sae.org/publications/technical-papers/content/2009-01-2890/. Number: 2009-01-2890.

[27] Drew Landman, Matthew Cragun, Mike McCormick, and Richard Wood. Drag Reduction of a Modern Straight Truck. *SAE International Journal of Commercial Vehicles*, 4(1):256–262, September 2011. doi: 10.4271/2011-01-2283. URL https://saemobilus.sae.org/articles/drag-reduction-a-modern-straight-truck-2011-01-2283. Publisher: SAE International.

[28] Marc Belzile, Jeff Patten, P Eng, Brian McAuliffe, William Mayda, and Bernard Tanguay. Technical Report Review of Aerodynamic Drag Reduction Devices for Heavy Trucks and Buses. *Project*, 54:A3578, 2012.

[29] G. M. R. Van Raemdonck and M. J. L. Van Tooren. Numerical and wind tunnel analysis together with road test of aerodynamic add-ons for trailers. In *International Conference on Engineering Conferences International*, pages 237–252. Springer, 2010.

[30] Michael Gerard Connolly, Alojz Ivankovic, and Malachy J. O'Rourke. A Novel Method for Evaluating on-Road Drag Changes Using Constant Power Measurements. SAE Technical Paper 2025-01-8764, SAE International, Warrendale, PA, April 2025. URL https://www.sae.org/publications/technical-papers/content/2025-01-8764/. ISSN: 0148-7191, 2688-3627.

[31] Lisa Ydrefors, Mattias Hjort, Sogol Kharrazi, Jenny Jerrelind, and Annika Stensson Trigell. Rolling resistance and its relation to operating conditions: A literature review. *Proceedings of the Institution of Mechanical Engineers, Part D: Journal of Automobile Engineering*, 235(12):2931–2948, October 2021. ISSN 0954-4070. doi: 10.1177/09544070211011089. URL https://doi.org/10.1177/09544070211011089. Publisher: IMECHE.

[32] Pavel Niederle. ssp537 golf gte.pdf (4.79 MB) - Repair manuals - English (EN), October 2024. URL https://en.volkswagenclub.net/manual_download.php?id=1740.

[33] VW USA Press Release. 2015 Volkswagen Golf GTI Mk7 (US-Spec). URL https://www.caricos.com/cars/v/vw/2015_volkswagen_golf_gti_us/.

[34] Detailed specs review of 2016 Citroen Berlingo Multispace BlueHDI 100 model for Europe, October 2024. URL https://www.automobile-catalog.com/car/2016/2227385/citroen_berlingo_multispace_bluehdi_100.html.

[35] Gary J. Page and Astrid Walle. Towards a Standardized Assessment of Automotive Aerodynamic CFD Prediction Capability - AutoCFD 2: Windsor Body Test Case Summary. SAE Technical Paper 2022-01-0898, SAE International, Warrendale, PA, March 2022. URL https://www.sae.org/publications/technical-papers/content/2022-01-0898/. ISSN: 0148-7191, 2688-3627.

[36] AutoCFD4 | AutoCFD5, . URL https://autocfd.org/autocfd4/.